

# Inhaltsverzeichnis

<b>1</b>	<b>Introduction</b>	<b>3</b>
1.1	FAIR project . . . . .	3
1.2	Beam transfer systems of the FAIR accelerator . . . . .	3
<b>2</b>	<b>Theoretical background</b>	<b>4</b>
2.1	Introduction of the bunch to bucket transfer . . . . .	4
2.1.1	Phase difference between two RF systems . . . . .	4
2.1.2	Synchronization of two RF systems . . . . .	4
2.1.2.1	Phase shift method . . . . .	4
2.1.2.1.1	Longitudinal dynamics analysis . . . . .	5
2.1.2.1.2	Transverse dynamics analysis . . . . .	5
2.1.2.1.3	Adiabaticity analysis . . . . .	5
2.1.2.2	$\phi_s(t)$ . . . . .	6
2.1.2.2.1	$d\phi_s(t)/dt$ . . . . .	6
2.1.2.3	Examples of RF frequency modulation for 200Mev $U^{28+}$ SIS18 . . . . .	6
2.1.2.4	Frequency beating method . . . . .	7
2.1.2.5	Longitudinal dynamics analysis 2-3 Seiten . . . . .	7
2.1.2.6	Example of frequency beating method for SIS18 and SIS100 1 Seite . . . . .	8
2.1.2.6.1	Frequency beating method for SIS18 and ESR 2-3 Seiten . . . . .	10
2.1.3	Bucket label . . . . .	10
2.1.4	Synchronization of the extraction and injection kicker . . . . .	10
2.1.5	Beam indication for the beam instrumentation . . . . .	10
2.2	Prerequisites/boundary conditions for the B2B transfer system . . . . .	10
2.2.1	LLRF system . . . . .	10
2.2.2	Accelerator control system . . . . .	10
2.2.2.1	BuTiS . . . . .	10
2.2.2.2	GMT . . . . .	10
2.2.2.3	FESA . . . . .	10
2.2.2.4	SM . . . . .	10
<b>3</b>	<b>First idea on the B2B transfer system</b>	<b>11</b>
3.1	Data acquisition from two synchrotrons . . . . .	11
3.2	Coarse synchronization . . . . .	11
3.3	Fine synchronization . . . . .	11

<b>4 Concept of the B2B transfer system</b>	<b>12</b>
4.1 Basic procedure of the B2B transfer system for FAIR . . . . .	12
4.2 Functional blocks and responsibilities . . . . .	12
<b>5 Realization and systematic investigation of the B2B transfer system</b>	<b>13</b>
5.1 Investigation from the beam dynamics view for the RF phase adjustment of $U^{28+}$ for SIS18 . . . . .	13
5.1.0.5 Longitudinal dynamic analysis for the simulation . . . . .	14
5.1.0.6 Transverse dynamics analysis for the simulations . . . . .	17
5.1.1 Longitudinal dynamics analysis of the frequency beating for SIS18 . . . . .	17
5.2 GMT systematic investigation for the B2B transfer system . . . . .	17
5.2.1 Calculation of the synchronization window and its uncertainty . . . . .	17
5.2.1.1 Synchronization window for the phase shift method and its uncertainty . . . . .	19
5.2.1.2 Synchronization window for the frequency beating method and its uncertainty . . . . .	21
5.2.2 WR network latency measurement . . . . .	22
5.3 Kicker systematic investigation for the B2B transfer system . . . . .	24
5.3.1 SIS18 extraction kicker units . . . . .	25
5.3.2 SIS100 injection kicker units . . . . .	25
5.4 Test setup for the data collection, merging and redistribution of the B2B transfer system . . . . .	27
5.4.1 Test requirement . . . . .	27
5.4.2 Test setup introduction . . . . .	28
5.4.3 Test result . . . . .	29
<b>6 Existing transfer system and the transfer system of the FAIR accelerators</b>	<b>32</b>
6.1 Existing transfer from SIS18 to ESR . . . . .	32
6.2 B2B transfer from SIS18 to ESR to CRYRING . . . . .	32
<b>7 Summary</b>	<b>33</b>
<b>8 Acknowledgement</b>	<b>34</b>
<b>9 References</b>	<b>35</b>
<b>A Formelzeichen</b>	<b>36</b>
A.1 Konstanten . . . . .	36
<b>B Messwerttabellen</b>	<b>37</b>
<b>C Abbildungsverzeichnis</b>	<b>38</b>

# Kapitel 1

## Introduction

1.1 FAIR project

1.2 Beam transfer systems of the FAIR accelerator

# Kapitel 2

## Theoretical background

### 2.1 Introduction of the bunch to bucket transfer

- Aufbau des Protoneninjektors, Nutzen, zu erreichende Werte, FAIR Vorgaben

#### 2.1.1 Phase difference between two RF systems

#### 2.1.2 Synchronization of two RF systems

The B2B transfer means that one bunch of particles, circulating inside the source synchrotron, is transferred into the center of a bucket of the target synchrotron. For the proper transfer, the phase advance between the bunch and the bucket must be precisely controlled before the bunch is ejected. The process of achieving the detailed phase adjustment is usually named as “synchronization”. There are usually two methods available for the synchronization process, the phase shift method and the frequency beating method. Both methods provide a time frame for the B2B transfer, within which a bunch could be transferred into a bucket with the center mismatch at least better than  $1^\circ$ . The time frame is called the synchronization window.

##### 2.1.2.1 Phase shift method

At a scheduled time well before ejection, the phase advance between the beam in the source synchrotron and a reference bucket in the target synchrotron are measured with respect to the phase of a common Synchronization Reference Signal, which is synchronously distributed to the source and target synchrotrons. Based on the measured phase advance, the Reference Radio Frequency (RF) Signals of the source or target or both synchrotrons are modulated away from their nominal value for a period of time and then modulated back so that the phase shift created by the frequency modulation could compensate for the expected phase difference. After the phase shift, the bunches of the source synchrotron are synchronized with the buckets of the target synchrotron. The phase shift process must be performed adiabatically for the longitudinal emittance to be preserved.

Fig. 1 shows the synchronization window for the phase shift method. The top and bottom RF signals are respectively from the source and target synchrotrons. For the phase shift method two RF signals are of the same frequency. The blue dots show the position of the bunches of the source synchrotron, the red dots correspond

to the bucket positions of the target synchrotron. The compensation of the time-of-flight is not drawn here. The red dashed line shows the end of the phase shift process and the beginning of the synchronization window, drawn in yellow. After the phase shift, bunches match with the corresponding buckets.

A particular case of the B2B synchronization occurs, when the target synchrotron is empty, i.e. it did not capture any bunch yet, the phase shift can be done for the target synchrotron without adiabatical consideration (e.g. Phase jump is possible).

### 2.1.2.1.1 Longitudinal dynamics analysis

We now consider how the radial position and momentum of the beam react when the RF frequency is changed from a nominal value. Since the magnetic field is not affected by the frequency change, we can assume  $\Delta B = 0$ ; then, eq. (??) and eq. (??) respectively reduce to

$$\frac{\Delta f}{f} = \left( \frac{\gamma_t^2}{\gamma^2} - 1 \right) \frac{\Delta R}{R} \quad (2.1)$$

$$\frac{\Delta f}{f} = \left( \frac{1}{\gamma^2} - \frac{1}{\gamma_t^2} \right) \frac{\Delta p}{p} \quad (2.2)$$

### 2.1.2.1.2 Transverse dynamics analysis

The momentum spread  $\Delta p/p \neq 0$  during the phase shift process causes chromaticity drift  $\Delta Q$ .  $Q$  is the chromaticity.

$$\Delta Q = Q \frac{\Delta p}{p} \quad (2.3)$$

### 2.1.2.1.3 Adiabaticity analysis

$\omega_s(t)$  is the small-amplitude synchrotron frequency given by

$$\omega_s(t) = \left[ -\frac{\eta(t) h \omega_{rev}^2(t) e V(t) \cos \phi_s(t)}{2\pi \beta^2(t) E(t)} \right]^{1/2} \quad (2.4)$$

A process is called “adiabatic” when the RF parameters are changed slowly enough for the longitudinal emittance to be preserved. The condition that the parameters are slowly varying can be expressed by

$$\varepsilon = \frac{1}{\omega_s^2(t)} \left| \frac{d\omega_s(t)}{dt} \right| \ll 1 \quad (2.5)$$

Compared with  $\phi_s(t)$ , all of the other variables change very slowly.  $\phi_s(t) = \phi_{s0}(t) + \Delta\phi_s(t)$ .  $\phi_{s0}(t)$  is the synchronous phase in the operation with no frequency modulation, and  $\Delta\phi_s(t)$  is the change in the synchronous phase, which originates from the frequency modulation. From Eq. (??) and Eq. (2.4), we can write the adiabaticity parameter  $\varepsilon$ , as follows:

$$\varepsilon \approx \frac{1}{2\omega_{s0}(t)} \left| \tan \phi_{s0}(t) \frac{d\phi_s(t)}{dt} \right| \quad (2.6)$$

Eq. (2.6) clearly shows that  $\phi_s(t)$  and  $d\phi_s(t)/dt$  play important roles for the adiabaticity when the frequency is modulated. Now let us deduce the the frequency requirement corresponding to these two factors.

### 2.1.2.2 $\phi_s(t)$

At the flattop, the bucket is a stationary bucket with  $\phi_s(t) = 0$ . During the frequency modulation process, the bucket becomes a running bucket with  $\Delta\phi_s(t) \neq 0$ . The ratio of bucket areas of a running bucket to a stationary bucket is bucket area factor  $\alpha(\phi_s)$ . Generally, the bucket area factor during the frequency modulation should be bigger than 80% in order for bunches to be preserved. A basic rf cavity requirement for beam acceleration rate is

$$V \sin\phi_s = 2\pi R_0 \rho \dot{B} \quad (2.7)$$

$$V \sin\phi_s = \frac{2\pi\rho_0}{\alpha_p} \left( \frac{R(t)}{R_0} \right)^{\frac{1}{\alpha_p}-1} B \dot{R} \quad (2.8)$$

$R(t)/R_0 \approx 1$ . From Eq. (2.1), we could get the following equation.

$$\frac{\dot{R}}{R_0} \left( \frac{\gamma_t^2}{\gamma^2} - 1 \right) = \frac{\dot{f}}{f_0} \quad (2.9)$$

substituting Eq. (2.9) into Eq. (2.8)

$$V \sin\phi_s = \frac{2\pi R_0 \rho B}{\left( \frac{1}{\gamma}^2 - \frac{1}{\gamma_t}^2 \right)} \frac{\dot{f}}{f} \quad (2.10)$$

The bucket area factor is determined by the synchronous phase change  $\Delta\phi_s$ . Based on Eq. (2.11), we know that  $\ddot{f}$  is important for the bucket size.

#### 2.1.2.2.1 $d\phi_s(t)/dt$

$$V \cos\phi_s \frac{d\phi_s}{dt} = \frac{2\pi R_0 \rho B}{\left( \frac{1}{\gamma}^2 - \frac{1}{\gamma_t}^2 \right)} \frac{\ddot{f}}{f} \quad (2.11)$$

Based on the adiabaticity Eq. (2.5),  $d\phi_s(t)/dt$  must be existing. So  $\ddot{f}$  must be existing. It means that  $\dot{f}$  must be continuous.

#### 2.1.2.3 Examples of RF frequency modulation for 200Mev $U^{28+}$ SIS18

To achieve a required phase shift, the RF frequency is modulated away from that required by the bending magnetic field. Let  $\Delta\phi$  be the phase shift to be achieved and  $\Delta f_{rf}(t)$  the RF frequency variation to accomplish it; then,

$$\Delta\phi = 2\pi \int_{t_0}^{t_0+T} \Delta f_{rf}(t) dt \quad (2.12)$$

where T is the period of frequency modulation and  $t_0$  is the time at which the modulation begins.

We have to introduce a phase shift of up to  $\pm\pi$  [rad] in the RF phase. This is the worstcase scenario, and in practice, the phase shift might be much less. We consider here the following four examples of frequency modulation; simple frequency-offset modulation (Case (1)), triangular modulation (Case (2)), sinusoidal modulation (Case (3)) and parabola modulation (Case (4)), (see Fig. 2.1(a)). Here we make use of

the maximum  $\dot{f}$  64 Hz/ms during the 1<sup>st</sup> stage of rf ramp to guarantee the 90% bucket area factor. Case (1)

$$\Delta f_{rf}(t) = \begin{cases} 50\text{Hz}/ms \times (t - t_0) & t_0 + 0 < t \leq t_0 + 2\text{ms} \\ 100\text{Hz} & t_0 + 2 < t \leq t_0 + 5\text{ms} \\ 100\text{Hz} - 50\text{Hz}/ms \times (t - t_0) & t_0 + 5\text{ms} < t \leq t_0 + 7\text{ms} \end{cases} \quad (2.13)$$

Case (2)

$$\Delta f_{rf}(t) = \begin{cases} \frac{10^3}{7 \times 3.5} \text{Hz}/ms \times (t - t_0) & t_0 + 0 < t \leq t_0 + 3.5\text{ms} \\ \frac{10^3}{7} \text{Hz} - \frac{10^3}{7 \times 3.5} \text{Hz}/ms \times (t - t_0 - 3.5\text{ms}) & t_0 + 3.5\text{ms} < t \leq t_0 + 7\text{ms} \end{cases} \quad (2.14)$$

Case (3)

$$\Delta f_{rf}(t) = \frac{10^3}{14} \text{Hz} \times (1 - \cos(\frac{2\pi}{7} \text{rad}/\text{ms} \times (t - t_0))) \quad t_0 + 0 < t \leq t_0 + 7\text{ms} \quad (2.15)$$

Case (4)

$$\Delta f_{rf}(t) = \begin{cases} 30\text{Hz}/ms^2 \times (t - t_0)^2 & t_0 + 0 < t \leq t_0 + 1\text{ms} \\ 30\text{Hz} + 60\text{Hz}/ms \times (t - t_0 - 1\text{ms}) & t_0 + 1\text{ms} < t \leq t_0 + 2.5\text{ms} \\ 30\text{Hz}/ms^2 \times [5\text{ms} - (t - t_0 - 3.5\text{ms})]^2 & t_0 + 2.5\text{ms} < t \leq t_0 + 4.5\text{ms} \\ 30\text{Hz} + 60\text{Hz}/ms \times (6\text{ms} - t - t_0) & t_0 + 4.5\text{ms} < t \leq t_0 + 6\text{ms} \\ 30\text{Hz}/ms^2 \times [7\text{ms} - (t - t_0)]^2 & t_0 + 6\text{ms} < t \leq t_0 + 7\text{ms} \end{cases} \quad (2.16)$$

All the four modulations realize the same phase shift  $\Delta\phi = 180^\circ$  (see Fig. 2.1(8) within T=7ms .

By Eq. (2.1) and Eq. (2.2) we could get the average radial excursion and relative momentum shift. (see Fig. 2.1(2) and Fig. 2.1(3)), which are much smaller than the maximum momentum modulation  $\pm 0.008$  and maximum radial excursion  $\pm 2.4 \times 10^{-4}$ . Fig. 2.1(6) shows the changes in synchronous phase caused by four RF frequency modulations.

#### 2.1.2.4 Frequency beating method

Einführung in die Arbeitsweise des 4-grids, . . .

#### 2.1.2.5 Longitudinal dynamics analysis 2-3 Seiten

For the frequency beating method, we guarantee the extraction and injection energy always match, which means that the momentum is not affected by the frequency change, namely  $\Delta p = 0$ ; then the general relation between the radial excursion and RF frequency change Eq. (2.20) reduces to Eq. (2.22) and the general relation between the magnetic field change and RF frequency change Eq. (2.21) reduces to Eq. (2.23).

$$\frac{\Delta f}{f} = -\frac{\Delta R}{R} \quad (2.17)$$

$$\frac{\Delta f}{f} = \frac{1}{\gamma_t^2} \times \frac{\Delta B}{B} \quad (2.18)$$

## 2.1. INTRODUCTION OF THE BUNCH TO BUCKET TRANSFER BACKGROUND

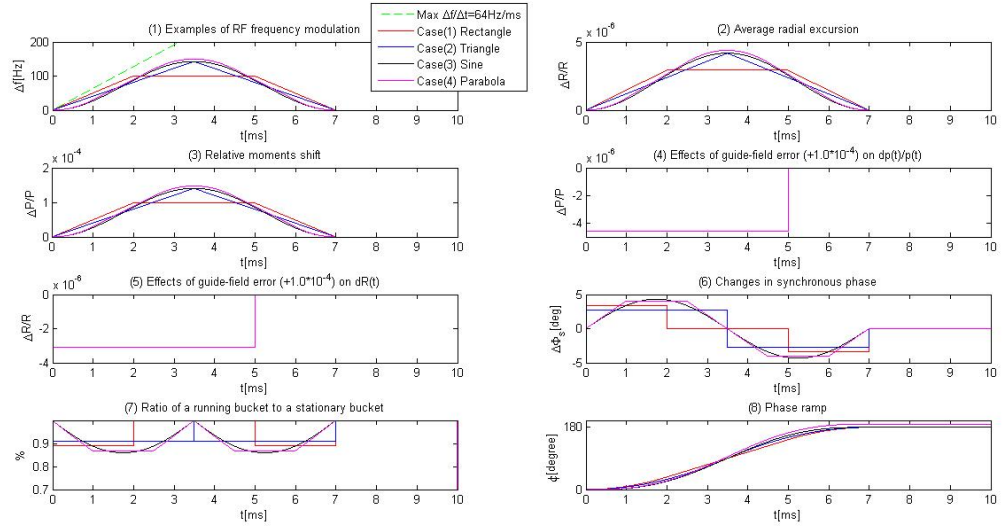


Abbildung 2.1: (1) RF frequency modulations, (2) average radial excursions, (3) relative momentum shifts, (4) effects of guide-field error on  $dp(t)/p(t)$ , (5) effects of guide-field error on  $dR(t)$ , (6) changes in synchronous phase, (7) ratio of a running bucket to a stationary bucket and (8) Phase ramp.

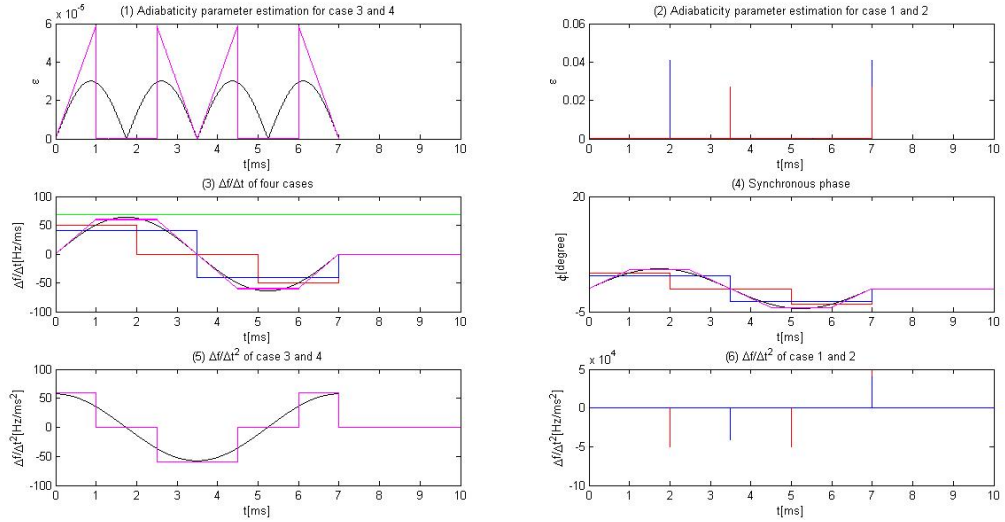


Abbildung 2.2: (1) Adiabaticity parameter estimation for case 3 and 4, (2) adiabaticity parameter estimation for case 1 and 2, (3)  $\dot{f}$  of four cases, (4) Synchronous phase, (5)  $\ddot{f}$  of case 3 and 4 and (6)  $\ddot{f}$  of case 1 and 2.

### 2.1.2.6 Example of frequency beating method for SIS18 and SIS100 1 Seite

Because the circumference ratio of the large machine to the small machine is a perfect integer, the rf frequency at the flattop of SIS18 is same as that of SIS100. So the first step for the bunch to bucket transfer is the RF frequency de-tune. In order to realize the frequency beating between two synchrotrons, the RF frequency of the source synchrotron or the target synchrotron or both synchrotrons can be de-tuned.

It means that the particles on the de-tuned synchrotron run at an average radius different by  $\Delta R$  from the designed orbit  $R$ . For the synchronization of the SIS18 and the SIS100, we will de-tune the RF frequency on the SIS18. The SIS18 operates with a cycle length of 520ms, harmonic number of 2 ( $h = 2$ ), and RF frequency of approximately 0.43 MHz at injection and approximately 1.57 MHz at ejection for the  $U^{28+}$  [?]. During nominal operation, the SIS18 forms two bunches from the beam injected at 11.4 MeV/ $\mu$  and accelerates them up to 200 MeV/ $\mu$ . From the SIS18, 4 batches, each of 2 bunches, are transferred at maximum 10ms intervals to the SIS100. The harmonic number of the SIS100 is 10 and the SIS100 RF frequency is fixed at approximately 1.57 MHz during the injection period to simplify the RF control system and to avoid perturbing batches already transferred.

This RF frequency de-tune is done accompanying with the RF ramp. Accepting to decentre the orbit by 8mm for the SIS18 [?]:

$$\frac{\Delta R}{R} \approx 2.4 \times 10^{-4} \quad (2.19)$$

We know the basic differential relations among the fractional change in the RF frequency  $f$ , the fractional change in the momentum  $p$ , the fractional change in the bending magnetic field  $B$  and the fractional change in the radius  $R$  as follows [?].

$$\frac{\Delta f}{f} = \frac{1}{\gamma^2} \frac{\Delta p}{p} - \frac{\Delta R}{R} \quad (2.20)$$

$$\frac{\Delta f}{f} = \left( \frac{1}{\gamma^2} - \frac{1}{\gamma_t^2} \right) \frac{\Delta p}{p} + \frac{1}{\gamma_t^2} \frac{\Delta B}{B} \quad (2.21)$$

where  $\gamma$  is the relativistic factor, which measures the total particle energy,  $E$ , in units of the particle rest energy,  $E_0$ ;  $\gamma_t$  is the transition gamma;  $\Delta f$  and  $\Delta B$  are the frequency and bending magnetic field deviation for the frequency de-tune;  $\Delta p$  is the momentum deviation.

In our case of the frequency beating method, we guarantee the extraction and injection energy always match, which means that the momentum is not affected by the frequency change, namely  $\Delta p = 0$ ; then the general relation between the radial excursion and RF frequency change Eq. (2.20) reduces to Eq. (2.22) and the general relation between the magnetic field change and RF frequency change Eq. (2.21) reduces to Eq. (2.23).

$$\frac{\Delta f}{f} = - \frac{\Delta R}{R} \quad (2.22)$$

$$\frac{\Delta f}{f} = \frac{1}{\gamma_t^2} \times \frac{\Delta B}{B} \quad (2.23)$$

From these equations, the RF frequency and the magnetic field change at the  $U^{28+}$  extraction energy 200MeV/u [?] ( $\gamma_t = 5.8$ ) are

$$\frac{\Delta f}{f} = -2.4 \times 10^{-4} \quad (2.24)$$

$$\frac{\Delta B}{B} = -8.1 \times 10^{-3} \quad (2.25)$$

where the maximum RF frequency de-tune is approximate to 370 Hz at 1.57 MHz for the  $U^{28+}$ . In this paper, we assume Rf frequency de-tune for the SIS18 equals to 200 Hz for the sake of simplicity. The beating period is 5ms.

#### **2.1.2.6.1 Frequency beating method for SIS18 and ESR 2-3 Seiten**

Because the circumference ratio of the ESR injection orbit to the SIS18 designed orbit is not a perfect integer, two machines begin beating automatically. He

#### **2.1.3 Bucket label**

#### **2.1.4 Synchronization of the extraction and injection kicker**

#### **2.1.5 Beam indication for the beam instrumentation**

### **2.2 Prerequisites/boundary conditions for the B2B transfer system**

- Aufbau des Protoneninjektors, Nutzen, zu erreichende Werte, FAIR Vorgaben

#### **2.2.1 LLRF system**

#### **2.2.2 Accelerator control system**

##### **2.2.2.1 BuTiS**

##### **2.2.2.2 GMT**

##### **2.2.2.3 FESA**

##### **2.2.2.4 SM**

# Kapitel 3

## First idea on the B2B transfer system

3.1 Data acquisition from two synchrotrons

3.2 Coarse synchronization

3.3 Fine synchronization

# Kapitel 4

## Concept of the B2B transfer system

- 4.1 Basic procedure of the B2B transfer system for FAIR
- 4.2 Functional blocks and responsibilities

# Kapitel 5

## Realization and systematic investigation of the B2B transfer system

### 5.1 Investigation from the beam dynamics view for the RF phase adjustment of $U^{28+}$ for SIS18

This section analyzes the phase shift and frequency beating methods from the beam-dynamics viewpoint for the synchronization of SIS18 with SIS100. In this chapter, the revolution frequency of SIS18 and SIS100 are denoted by  $f_{h=1}^{SIS18}$  and  $f_{h=1}^{SIS100}$  and the RF frequency by  $f_{h=2}^{SIS18}$  and  $f_{h=10}^{SIS100}$ . Since SIS18 and SIS100 harmonic number is 2 and 10, the relationship between these frequencies is  $f_{h=2}^{SIS18} = 2f_{h=1}^{SIS18}$  and  $f_{h=10}^{SIS100} = 10f_{h=1}^{SIS100}$ .

To achieve a required phase shift, the RF frequency is modulated away from that required by the bending magnetic field or the guide field. Let  $\Delta\phi_{shift}$  be the phase shift to be achieved and  $\Delta f(t)$  the RF frequency variation to accomplish it; then,

$$\Delta\phi_{shift} = 2\pi \int_{t_1}^{t_1+T} \Delta f(t) dt \quad (5.1)$$

where T is the period of frequency modulation and  $t_1$  is the time at which the modulation begins. To make the frequency modulation effective, the radial loop must be turned off just before the modulation begins.

I consider here the following four examples of frequency modulation; rectangle modulation (Case (1)), triangular modulation (Case (2)), biased sinusoidal modulation (Case (3)) and parabola modulation (Case (4)). All of these manipulations must be performed adiabatically. So I make use the maximum time derivative of rf frequency f during the acceleration ramp as the reference,  $df/dt=64\text{Hz}/\text{ms}$ . Here we assume the phase shift must be achieved within 7ms. These frequency modulations are shown in Fig. ???. All the four modulations give the same phase shift,  $\Delta\phi_{shift} = \pi$ , which is proved by substituting each form of  $\Delta f(t)$  into eq. 5.1 and performing integration. Fig. 5.2 shows the time derivation of four rf frequency modulations.

Case (1)

$$\Delta f(t) = \begin{cases} 50(t - t_1), & t_1 < t \leq t_1 + 2ms \\ 100, & t_1 + 2ms < t \leq t_1 + 5ms \\ -50(t - t_1) + 7 \times 50, & t_1 + 5ms < t \leq t_1 + 7ms \end{cases} \quad (5.2)$$

Case (2)

$$\Delta f(t) = \begin{cases} \frac{500}{3.5 \times 3.5}(t - t_1), & t_1 < t \leq t_1 + 3.5ms \\ -\frac{500}{3.5 \times 3.5}(t - t_1) + 7 \times \frac{500}{3.5 \times 3.5}, & t_1 + 3.5ms < t \leq t_1 + 7ms \end{cases} \quad (5.3)$$

Case (3)

$$\Delta f(t) = \frac{1000}{7 \times 2}(1 - \cos(\frac{2\pi}{7} \times (t - t_1))), \quad t_1 < t \leq t_1 + 7ms \quad (5.4)$$

Case (4)

$$\Delta f(t) = \begin{cases} 30(t - t_1)^2, & t_1 < t \leq t_1 + 1ms \\ 30 + 60((t - t_1) - 1), & t_1 + 1ms < t \leq t_1 + 2.5ms \\ 30(5 - ((t - t_1) - 3.5)^2), & t_1 + 2.5ms < t \leq t_1 + 4.5ms \\ 30 + 60(6 - (t - t_1)), & t_1 + 4.5ms < t \leq t_1 + 6ms \\ 30(7 - (t - t_1))^2, & t_1 + 6ms < t \leq t_1 + 7ms \end{cases} \quad (5.5)$$

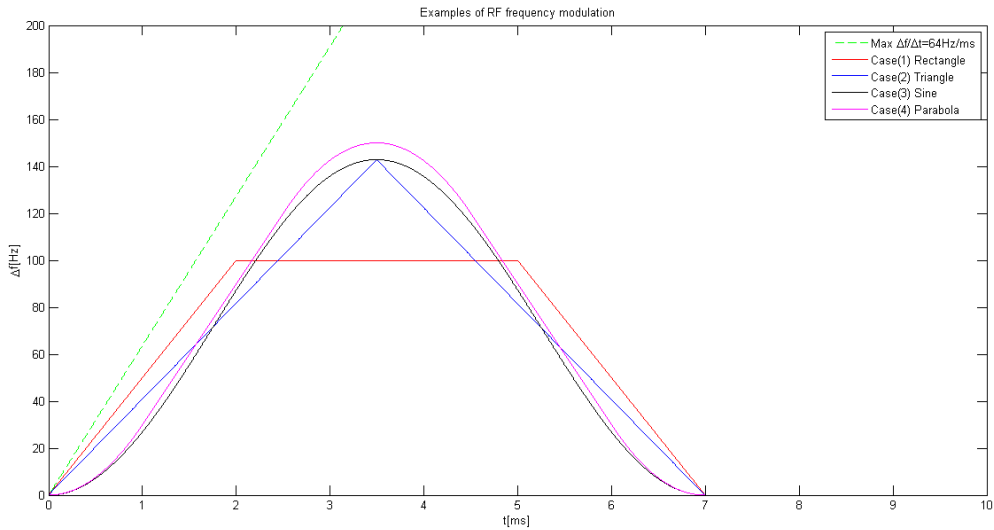


Abbildung 5.1: Examples of RF frequency modulation.

### 5.1.0.5 Longitudinal dynamic analysis for the simulation

- Average radial excursion and the relative momentum shift

The average radial excursion and the relative momentum shift are calculated for the four kinds of RF frequency modulations by eq. (2.1) and eq. (2.2), see Fig. ??(a) and Fig. ??(b). The momentum modulation and radial excursion of four cases are much smaller than the maximum momentum modulation  $\pm 0.008$  and maximum radial excursion  $\pm 2.4 \times 10^{-4}$  of SIS18.

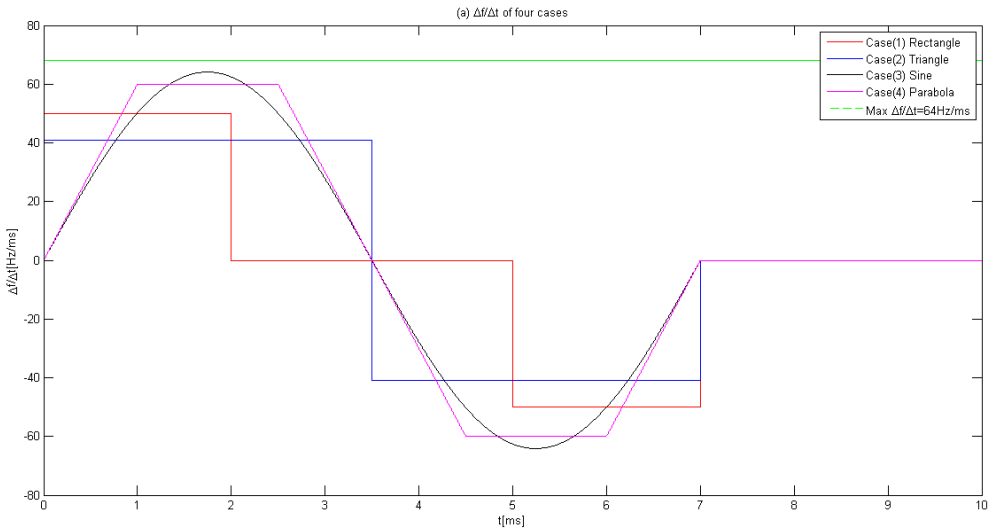


Abbildung 5.2: Time derivation of four modulations

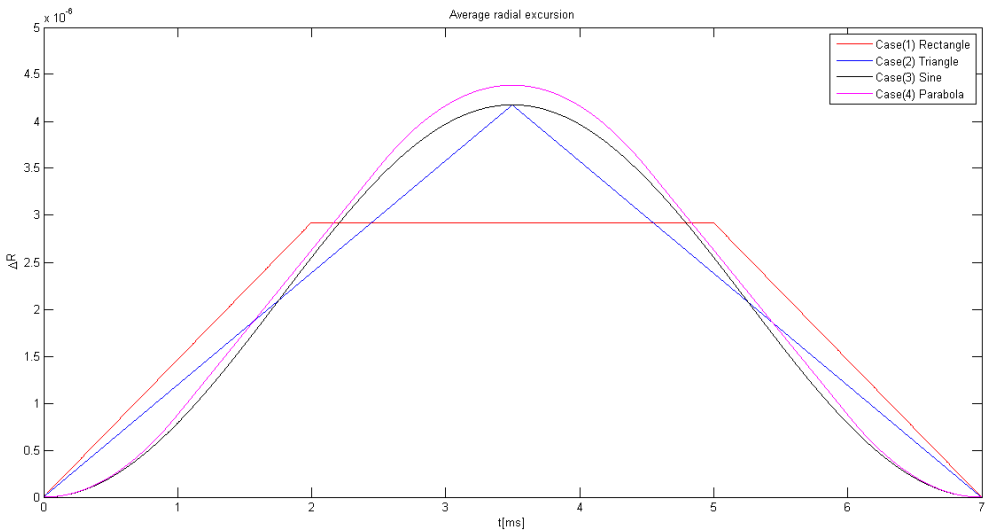


Abbildung 5.3: Average radial excursions for four cases.

- Synchronous phase

The rf frequency modulations make the synchronous phase deviate from the original one. Fig. 5.5 shows the changes in synchronous phase,  $\Delta\phi_s(t)$ , caused by RF frequency modulations for four cases, calculated by introducing values into eq. (??). For case (1), jumps in  $\Delta\phi_s(t)$  appear at the start and end of the frequency modulation, and at two points where the slope of modulation changes from upward to flat and from flat to downward. For case (2), jumps in  $\Delta\phi_s(t)$  appear at the start and end of the frequency modulation, and at the midpoint where the slope of modulation changes from upward to downward. The jumps in  $\Delta\phi_s(t)$  are dangerous for beam to follow. For case (3) and (4), the synchronous phase  $\Delta\phi_s(t)$  during the modulations are continuous.

- Bucket size

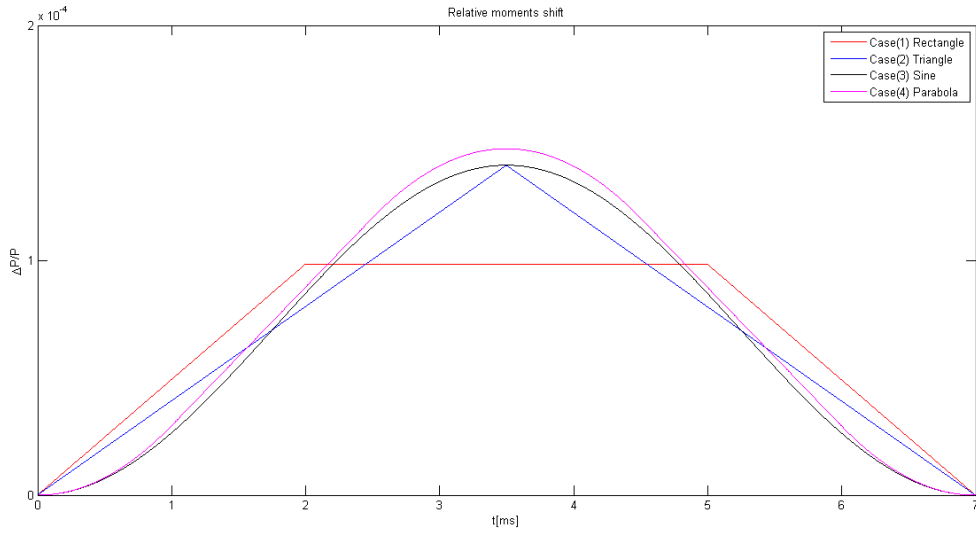


Abbildung 5.4: Relative momentum shifts for four cases.

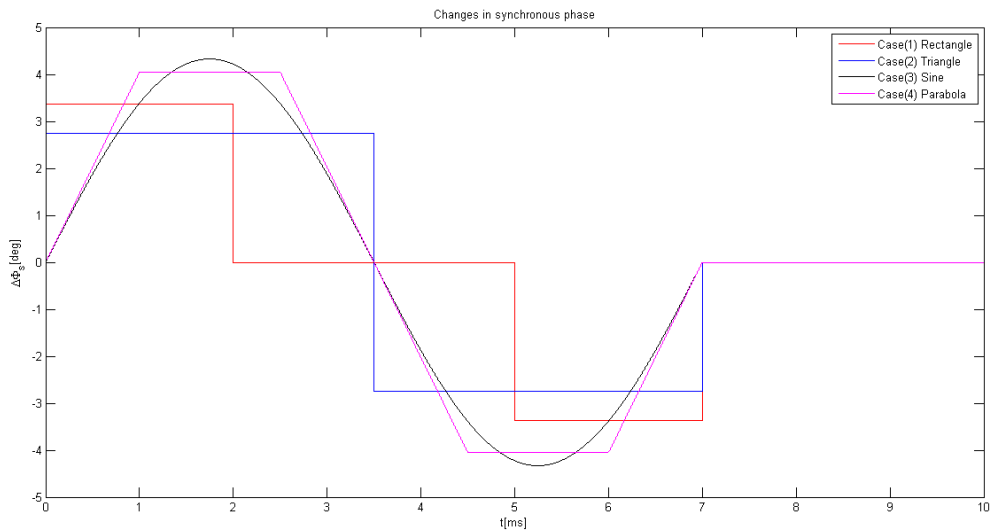


Abbildung 5.5: Changes in synchronous phase caused by RF frequency modulations for four cases

The bucket area factor  $\alpha_b(\phi_s)$  varies during rf frequency modulations. Before the modulations, the synchronous phase  $\phi_s = 0^\circ$  and  $\alpha_b(0^\circ) = 1$ . By introducing the changes in synchronous phase into eq. (5.6), we get the ratio of bucket areas for four cases, see Fig. (5.6). Four rf frequency modulations have the bucket area factor better than 85%.

$$\alpha_b(\phi_s) \approx (1 - \sin\phi_s)(1 - \sin\phi_s) \quad (5.6)$$

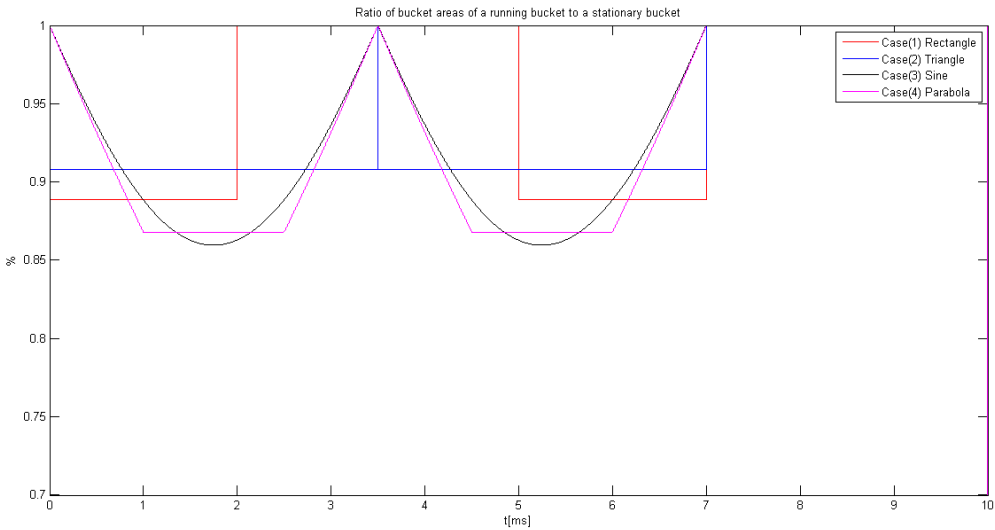


Abbildung 5.6: Ratio of bucket areas of a running bucket to the stationary bucket for four cases

#### 5.1.0.6 Transverse dynamics analysis for the simulations

#### 5.1.1 Longitudinal dynamics analysis of the frequency beating for SIS18

-technische Daten (Länge, Durchmesser,...) - Strahlführungskomponenten –Solenoid-Steerer-Kombination (Funktion, Platzierung, Aufbau)

## 5.2 GMT systematic investigation for the B2B transfer system

### 5.2.1 Calculation of the synchronization window and its uncertainty

Principally speaking, the synchronization window is a time frame within which the bunch could be injected into the bucket with the bunch to bucket center mismatch better than  $1^\circ$ . In fact, we need just two SIS100 revolution periods long, achieving much preciser injection. The ideal beginning of the synchronization window denotes by  $WIN_{start}$ . The synchronization window is within the range  $[WIN_{start}, WIN_{start} + 2 \times T_{rev}^{SIS100}]$ .  $T_{rev}^{SIS100}$  is the revolution period of SIS100, which equals to 6.359 us for U<sup>28+</sup> at 200Mev/u. The uncertainties in the phase prediction and rf cavity frequency cause an uncertainty  $\delta WIN_{start}$  to the  $WIN_{start}$ . The rf cavity harmonic of SIS18 is 2 and that of SIS100 is 10. The Phase advance prediction module extrapolates the rf phase  $\psi_{h=1}^{SIS100}$  for SIS100 rf h=1 signal and  $\psi_{h=1/5}^{SIS18}$  for SIS18 rf h=1/5 signal at  $t_\psi$ . The phase prediction needs 500us. More details about the phase advance measurement and phase advance prediction modules, please see Tibo's thesis. Fig. 5.7 illustrates some basic definition of symbols for the calculation.  $\phi_{h=2}^{SIS18}$  and  $\phi_{h=10}^{SIS100}$  are individual rf phase of SIS18 and SIS100 rf reference signals at  $t_\psi$ . The relationship between

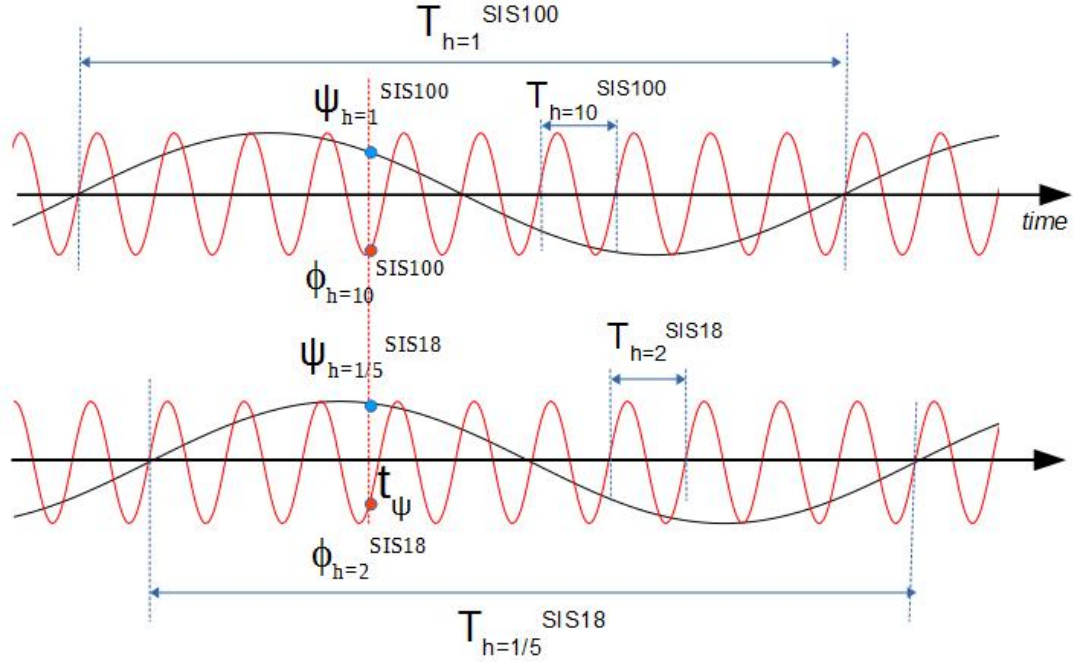


Abbildung 5.7: The illustration of symbols for SIS100

$\phi_{h=2}^{SIS18}$ ,  $\phi_{h=10}^{SIS100}$  and  $\psi_{h=1/5}^{SIS18}$ ,  $\psi_{h=1}^{SIS100}$  are given by eq. 5.10 and eq. 5.9. The uncertainty of  $\psi_{h=1/5}^{SIS18}$  and  $\psi_{h=1}^{SIS100}$  is  $0.05^\circ$ .

$$\phi_{h=2}^{SIS18} = \frac{\frac{\psi_{h=1/5}^{SIS18}}{360^\circ} \times T_{h=1/5}^{SIS18} \bmod T_{h=2}^{SIS18}}{T_{h=2}^{SIS18}} \times 360^\circ \quad (5.7)$$

$$\phi_{h=10}^{SIS100} = \frac{\frac{\psi_{h=1}^{SIS100}}{360^\circ} \times T_{h=1}^{SIS100} \bmod T_{h=10}^{SIS100}}{T_{h=10}^{SIS100}} \times 360^\circ \quad (5.8)$$

substituting  $T_{h=2}^{SIS18} \times 10 = T_{h=1/5}^{SIS18}$ ,  $T_{h=10}^{SIS100} \times 10 = T_{h=1}^{SIS100}$  into eq.5.9 and eq.5.10 yields

$$\phi_{h=2}^{SIS18} = \frac{\frac{\psi_{h=1}^{SIS18} \times 10}{360^\circ} \times T_{h=2}^{SIS18} \bmod T_{h=2}^{SIS18}}{T_{h=2}^{SIS18}} \times 360^\circ \quad (5.9)$$

$$\phi_{h=10}^{SIS100} = \frac{\frac{\psi_{h=1}^{SIS100} \times 10}{360^\circ} \times T_{h=10}^{SIS100} \bmod T_{h=10}^{SIS100}}{T_{h=10}^{SIS100}} \times 360^\circ \quad (5.10)$$

The uncertainty of  $\phi_{h=2}^{SIS18}$  and  $\phi_{h=10}^{SIS100}$  are

$$\delta\phi_{h=2}^{SIS18} = \sqrt{\left(\frac{\partial\phi_{h=2}^{SIS18}}{\partial\psi_{h=2}^{SIS18}}\delta\psi_{h=2}^{SIS18}\right)^2} = \sqrt{(10 \times \delta\psi_{h=2}^{SIS18})^2} = 0.5^\circ \quad (5.11)$$

$$\delta\phi_{h=10}^{SIS100} = \sqrt{\left(\frac{\partial\phi_{h=10}^{SIS100}}{\partial\psi_{h=10}^{SIS100}}\delta\psi_{h=10}^{SIS100}\right)^2} = \sqrt{(10 \times \delta\psi_{h=10}^{SIS100})^2} = 0.5^\circ \quad (5.12)$$

When we change the uncertainty of  $\phi_{h=2}^{SIS18}$  and  $\phi_{h=10}^{SIS100}$  at  $t_\psi$  from phase to time domain. The uncertainty of  $t_\psi$  is

$$\delta t_\psi = \frac{\delta\phi_{h=2}^{SIS18}}{360^\circ} \times \frac{1}{157KHz} = \frac{0.05^\circ}{360^\circ} \times \frac{1}{157KHz} \approx 1ns \quad (5.13)$$

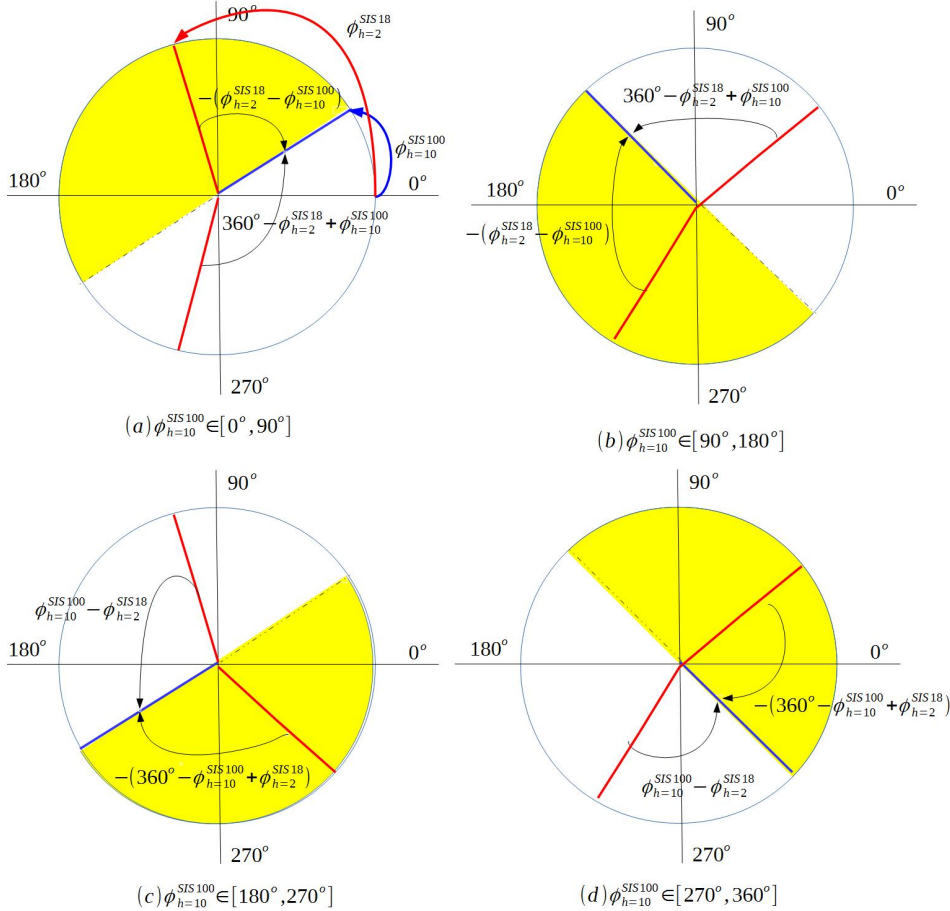


Abbildung 5.8: Scenarios for the phase shift method

### 5.2.1.1 Synchronization window for the phase shift method and its uncertainty

Different relation between  $\phi_{h=2}^{SIS18}$  and  $\phi_{h=10}^{SIS100}$  has different required phase adjustment for SIS18. Fig. 5.8 illustrates all scenarios of their relation and the required phase adjustment for each scenario. The blue and red line represents the phase of SIS100 and SIS18 rf reference signal. The clockwise arrow from the SIS18 to SIS100 rf phase represents the negative phase adjustment for SIS18, and the anticlockwise represents the positive phase adjustment for SIS18. The required phase adjustment of SIS18 is denoted by  $\Delta\phi_{shift}$ .

- $\phi_{h=10}^{SIS100} \in [0, 90^\circ]$ , see Fig. 5.9 (a).

- $\phi_{h=10}^{SIS100} < \phi_{h=2}^{SIS18} < \phi_{h=10}^{SIS100} + 180^\circ$ , which denotes by the yellow semicircle in Fig. 5.9 (a).

$$\Delta\phi_{shift} = -(\phi_{h=2}^{SIS18} - \phi_{h=10}^{SIS100}) \quad (5.14)$$

- $\phi_{h=2}^{SIS18} < \phi_{h=10}^{SIS100}$  or  $\phi_{h=2}^{SIS18} > \phi_{h=10}^{SIS100} + 180^\circ$ , which denotes by the white semicircle in Fig. 5.9 (a).

$$\Delta\phi_{shift} = 360^\circ - \phi_{h=2}^{SIS18} + \phi_{h=10}^{SIS100} \quad (5.15)$$

- $\phi_{h=10}^{SIS100} \in [90, 180^\circ]$ , see Fig. 5.9 (b).

- $\phi_{h=2}^{SIS18} < \phi_{h=10}^{SIS100}$  or  $\phi_{h=2}^{SIS18} > \phi_{h=10}^{SIS100} + 180^\circ$ , which denotes by the yellow semicircle in Fig. 5.9 (b).

$$\Delta\phi_{shift} = -(\phi_{h=2}^{SIS18} - \phi_{h=10}^{SIS100}) \quad (5.16)$$

- $\phi_{h=10}^{SIS100} < \phi_{h=2}^{SIS18} < \phi_{h=10}^{SIS100} + 180^\circ$ , which denotes by the white semicircle in Fig. 5.9 (b).

$$\Delta\phi_{shift} = 360^\circ - \phi_{h=2}^{SIS18} + \phi_{h=10}^{SIS100} \quad (5.17)$$

- $\phi_{h=10}^{SIS100} \in [180, 270^\circ]$ , see Fig. 5.9 (c).

- $\phi_{h=2}^{SIS18} > \phi_{h=10}^{SIS100}$  or  $\phi_{h=2}^{SIS18} < \phi_{h=10}^{SIS100} + 180^\circ - 360^\circ$ , which denotes by the yellow semicircle in Fig. 5.9 (c).

$$\Delta\phi_{shift} = -(360^\circ - \phi_{h=10}^{SIS100} + \phi_{h=2}^{SIS18}) \quad (5.18)$$

- $\phi_{h=10}^{SIS100} - 180^\circ < \phi_{h=2}^{SIS18} < \phi_{h=10}^{SIS100}$ , which denotes by the white semicircle in Fig. 5.9 (c).

$$\Delta\phi_{shift} = \phi_{h=10}^{SIS100} - \phi_{h=2}^{SIS18} \quad (5.19)$$

- $\phi_{h=10}^{SIS100} \in [270, 360^\circ]$ , see Fig. 5.9 (d).

- $\phi_{h=10}^{SIS100} - 180^\circ < \phi_{h=2}^{SIS18} < \phi_{h=10}^{SIS100}$ , which denotes by the yellow semicircle in Fig. 5.9 (d).

$$\Delta\phi_{shift} = -(360^\circ - \phi_{h=10}^{SIS100} + \phi_{h=2}^{SIS18}) \quad (5.20)$$

- $\phi_{h=2}^{SIS18} > \phi_{h=10}^{SIS100}$  or  $\phi_{h=2}^{SIS18} < \phi_{h=10}^{SIS100} + 180^\circ - 360^\circ$ , which denotes by the white semicircle in Fig. 5.9 (d).

$$\Delta\phi_{shift} = \phi_{h=10}^{SIS100} - \phi_{h=2}^{SIS18} \quad (5.21)$$

The phase adjustment is achieved by the phase shift method within the upper bound time,  $T_{phase\text{shift}}^{upperbound}$ . For the  $U^{28}$  B2B transfer from SIS18 to SIS100,  $T_{phase\text{shift}}^{upperbound}$  equals to 7ms. The phase shift  $\Delta\phi_{shift}$  is achieved within 7ms. The beginning of the synchronization window is expressed by

$$WIN_{start} = t_\psi - 500\mu s + T_{phase\text{shift}}^{upperbound} \quad (5.22)$$

The uncertainty in the phase prediction  $\psi_{h=1/5}^{SIS18}$  and  $\psi_{h=1}^{SIS100}$  equals to the uncertainty of  $t_\psi$ ,  $\delta t_\psi = 1\text{ns}$ . The phase shift uncertainty  $\delta\Delta\phi_{phase}$  equals to the uncertainty in the phase shift upper bound time,  $\delta T_{phaseshift}^{upperbound} = 100\text{ps}$ . Both causes an uncertainty in the  $WIN_{start}$ .

$$\begin{aligned}\delta WIN_{start} &= \sqrt{\left(\frac{\partial WIN_{start}}{\partial t_\psi} \delta t_\psi\right)^2 + \left(\frac{\partial WIN_{start}}{\partial T_{phaseshift}^{upperbound}} \delta T_{phaseshift}^{upperbound}\right)^2} \\ &= \sqrt{(\delta t_\psi)^2 + (T_{phaseshift}^{upperbound})^2} = \sqrt{1\text{ns}^2 + 100\text{ps}^2} = 1\text{ns}\end{aligned}\quad (5.23)$$

The synchronization window uncertainty of the phase shift method could be negligible. So the synchronization window is  $[WIN_{start}, WIN_{start} + 2 * 6.359\text{us}]$  for  $U^{28+}$  B2B transfer from SIS18 to SIS100.

### 5.2.1.2 Synchronization window for the frequency beating method and its uncertainty

Fig. 5.9 illustrates two scenarios for the frequency beating method. The frequency beating method can only achieve positive phase adjustment, which is denoted by  $\Delta\phi_{adjustment}$ .  $\Delta t$  is the beating time.

$$\Delta t = \frac{\Delta\phi_{adjustment}}{360^\circ \times \Delta f} \quad (5.24)$$

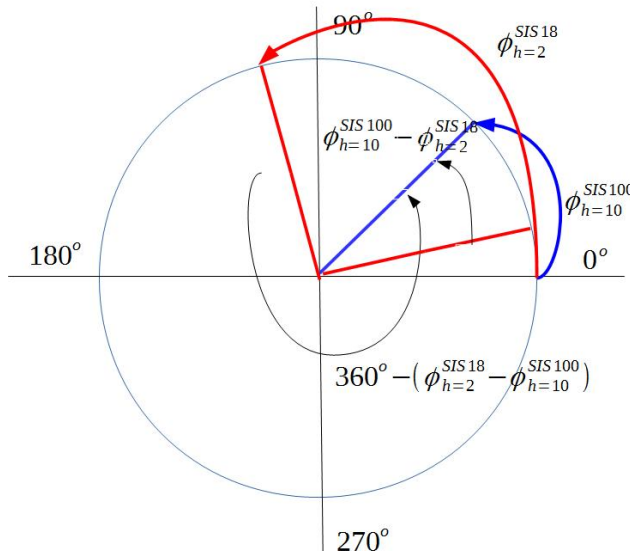


Abbildung 5.9: Two scenarios for the frequency beating method

- $\phi_{h=2}^{SIS18} \geq \phi_{h=10}^{SIS100}$
- $$\Delta\phi_{adjustment} = \phi_{h=10}^{SIS100} - \phi_{h=2}^{SIS18} \quad (5.25)$$

Replacing  $\Delta\phi_{adjustment}$  in eq. 5.29 with eq. 5.25, we have

$$\Delta t = \frac{\phi_{h=10}^{SIS100} - \phi_{h=2}^{SIS18}}{360^\circ \times \Delta f} \quad (5.26)$$

$$WIN_{start} = t_\psi - 500\mu s + \Delta t = t_\psi - 500\mu s + \frac{\phi_{h=10}^{SIS100} - \phi_{h=2}^{SIS18}}{360^\circ \times \Delta f} \quad (5.27)$$

- $\phi_{h=2}^{SIS18} < \phi_{h=10}^{SIS100}$

$$\Delta\phi_{adjustment} = 360^\circ - (\phi_{h=2}^{SIS18} - \phi_{h=10}^{SIS100}) \quad (5.28)$$

Replacing  $\Delta\phi_{adjustment}$  in eq. 5.29 with eq. 5.28, we have

$$\Delta t = \frac{360^\circ - (\phi_{h=2}^{SIS18} - \phi_{h=10}^{SIS100})}{360^\circ \times \Delta f} \quad (5.29)$$

$$WIN_{start} = t_\psi - 500\mu s + \Delta t = t_\psi - 500\mu s + \frac{360^\circ - (\phi_{h=2}^{SIS18} - \phi_{h=10}^{SIS100})}{360^\circ \times \Delta f} \quad (5.30)$$

Based on these two scenarios, we could deduce the formulas for the start of the synchronization window.

$$WIN_{start} = t_\psi - 500\mu s + \Delta t = t_\psi - 500\mu s + \frac{\Delta n \times 360^\circ - (\phi_{h=2}^{SIS18} - \phi_{h=10}^{SIS100})}{360^\circ \times \Delta f} \quad (5.31)$$

where  $\Delta n$  equals 1 when  $\phi_{h=2}^{SIS18} < \phi_{h=10}^{SIS100}$  and equals 0 when  $\phi_{h=2}^{SIS18} \geq \phi_{h=10}^{SIS100}$ . The uncertainties in the phase prediction and rf frequency detune cause an uncertainty in the WINstart.  $\delta\Delta f$  is  $\pm 38\text{Hz}$ , 24ppm.  $\delta\phi_{h=2}^{SIS18}$  and  $\delta\phi_{h=10}^{SIS100}$  are  $0.5^\circ$ .  $\Delta f$  is 200Hz. The maximum  $\Delta n \times 2\pi - (\phi_{h=2}^{SIS18} - \phi_{h=10}^{SIS100})$  is  $2\pi$ .

$$\begin{aligned} \delta WIN_{start} &= \sqrt{\left(\frac{\partial WIN_{start}}{\partial \phi_{h=2}^{SIS18}} \delta \phi_{h=2}^{SIS18}\right)^2 + \left(\frac{\partial WIN_{start}}{\partial \phi_{h=10}^{SIS100}} \delta \phi_{h=10}^{SIS100}\right)^2 + \left(\frac{\partial WIN_{start}}{\partial \Delta f} \delta \Delta f\right)^2} \\ &= \sqrt{\left(\frac{-1}{2\pi \times \Delta f} \delta \phi_{h=2}^{SIS18}\right)^2 + \left(\frac{1}{2\pi \times \Delta f} \delta \phi_{h=10}^{SIS100}\right)^2 + \left(-\frac{\Delta n \times 2\pi - (\phi_{h=2}^{SIS18} - \phi_{h=10}^{SIS100})}{2\pi \times \Delta f^2} \delta \Delta f\right)^2} \\ &\leq \sqrt{\left(\frac{-1}{2\pi \times 200} 0.5^\circ\right)^2 + \left(\frac{1}{2\pi \times 200} 0.5^\circ\right)^2 + \left(-\frac{2\pi}{2\pi \times 200^2} 38\right)^2} \\ &\approx 1\mu s \end{aligned} \quad (5.32)$$

So the synchronization window is  $[WIN_{start} - 1\mu s, WIN_{start} - 1\mu s + 2 * 6.359\mu s]$ .

### 5.2.2 WR network latency measurement

In this thesis, WR network latency measurement is achieved by the Xena traffic generator, which offers a new class of professional Layer 2-3 Gigabit Ethernet test platform. It performs high-precision performance measurement of throughput, latency, jitter, loss, sequence and mis-ordering errors.

Measurement setup is shown in Fig. 5.10. One Xena traffic generator is used in order to measure frame latency, jitter and packet loss for WR switches. For the measurements, Xena traffic generator sends the traffic streams with a unique stream ID for identifying latency, jitter and packet loss. A Virtual Local Area Network (VLAN) is a group of FECs in the WR network that is logically segmented by function or application, without regard to the physical locations of the FECs. For the WR network for FAIR, four VLANs are applied.

- DM VLAN
  - All FECs in the WR network are assigned to the DM broadcast VLAN, within which the DM forwards broadcast timing telegrams downwards to all FECs. The available average bandwidth for this VLAN corresponds to a rate of 100 Mbit/s. But the traffic is not evenly distributed across all destinations. DM bursts 60 messages at the ahead interval 500μs of a message schedule. Burst is a group of consecutive packets with shorter interpacket gaps than packets arriving before or after the burst of packets. The burst speed is 12 packets per 100μs.
  - The telegrams sent from the source B2B SCU upwards to the DM are unicast packets within DM unicast VLAN. 2 packets are send within 10 millisecond synchronization period. The maximum repetition frequency is 2.82Hz, the  $U^{28+}$  supercycle. So the average bandwidth is 6 packets per second. Besides, DM sends 10Mbps unicast traffic to FECs at the burst speed of 3 packets per 300μs.
- B2B VLAN. All SCUs for the B2B transfer are assigned to the B2B VLAN. The specified VLAN for the B2B transfer could reduce the traffic of the WR network. All B2B related broadcast telegrams are broadcasted in this VLAN. 100 packets are send within 10 millisecond synchronization period. The average bandwidth is 28 packets per second
- Low priority VLAN. This VLAN is used for the ... The available average bandwidth for this VLAN corresponds to a rate of 10 Mbps.

In Fig. 5.10, the port connected with the red optical fiber sends packets in the DM VLAN, the port connected with the yellow optical fiber sends packets in the B2B VLAN, and the port connected with the blue optical fiber sends packets in the low priority VLAN. Xena traffic generator sends traffic only directly to the 1st WR switch. Other three WR switches get traffic sequentially from their top layer WR switch. All WR switches send packets back to Xena traffic generator via the black connection, which achieves the latency, jitter and packet loss measurement for each layer switch. The length of all optical fiber in the test is 5 meter, whose latency could be ignored. Because the latency of the optical fiber with 1310 nm wavelength is about  $204 \text{ m}/\mu\text{s}$ . The latency for 5 meters is about 25ns.

Table 5.1 shows the packet latency and jitter measurement result of different layer WR switches. The test lasts for 17 hours and there exists no packet loss.

For the B2B transfer system, the maximum delay for the B2B related packets in the B2B VLAN and DM unicast VLAN is 500μs. The delay is decided by the number of WR switches and the length of the optical fiber. Even for 2km the delay is only about 10 μs. So the number of WR switches plays a more important role in the delay. Maximum 10 WR switches are available between the B2B source SCU and B2B target SCU, between B2B source SCU and source trigger SCU and between B2B source SCU and target trigger SCU and maximum 10 WR switches are available between the B2B source SCU and DM.

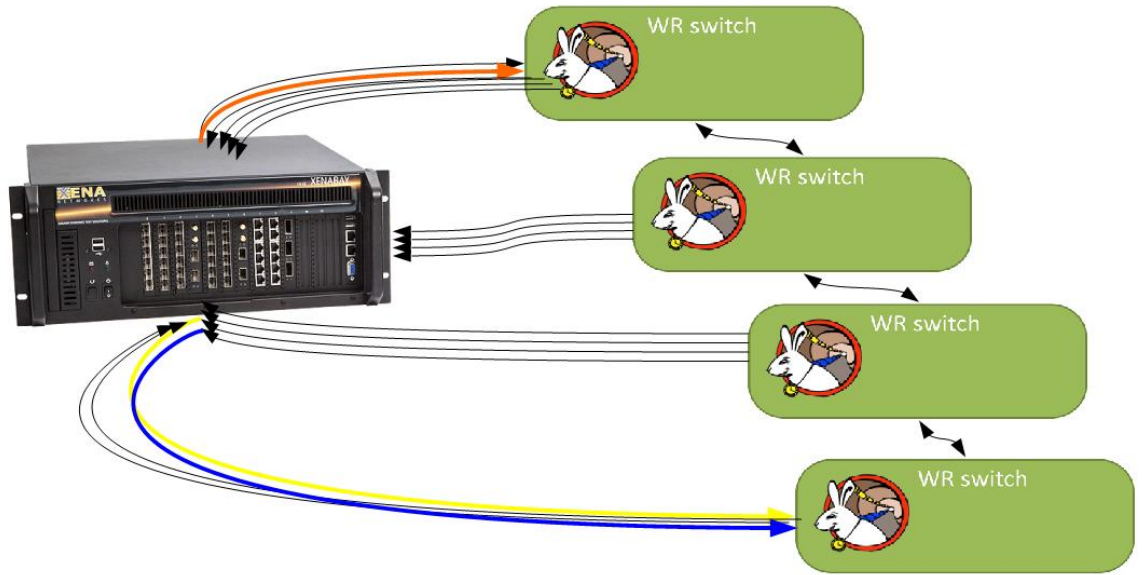


Abbildung 5.10: Schematic of the network setup

Tabelle 5.1: The latency of the WR switch

Number of WR switches	DM broadcast VLAN Max delay ± jitter	DM unicast VLAN Max delay ± jitter	B2B VLAN Max delay ± jitter	Low priority Max delay ± jitter
1	16.270us±13.590us	16.126us±13.398us	29.816us±27.109us	33.838us±31
2	17.825us±13.807us	17.825us±13.590us	32.074us±27.157us	38.320us±33
3	20.688us±13.951us	20.616us±13.783us	34.792us±27.133us	40.845us±32
4	23.502us±14.192us	23.358us±13.879us	38.167us±26.722us	44.526us±32

### 5.3 Kicker systematic investigation for the B2B transfer system

The SIS18 extraction kicker consists of 9 kicker units. In the existing topology, 5 kicker units are installed in the 1st crate and the other 4 units are in the 2nd crate. The width of each kicker unit is 0.25m and the distance between two kicker units is 0.09m. The distance between two crates is 19.167m. SIS100 injection kicker consists of 6 kicker units, which are equally located. The width of each kicker unit is 0.22m and the distance between two units is 0.23m. For the B2B transfer, the rise time of SIS18 extraction kicker and SIS100 injection kicker unit are 90ns and 1/20 of the revolution period. The rise time of these kickers must fit within the bunch gap, 25% of rf reference period. Here we are discussing about the following possibilities.

- For SIS18, whether the kicker units in the 2nd crate could be fired a fixed delay after the firing of the kicker units in the 1st crate for ion beams over the whole range of stable isotopes.
- For SIS100, whether the kicker units could be fired instantaneously.

Tabelle 5.2: The delay for firing two crates of SIS18 extraction kicker

Beam	$\beta$	time $L/\beta c$	bunch gap $G$	minimum delay $L/\beta c-G+90\text{ns}$	delay $D/\beta c$	maximum delay $G+d/\beta c-90\text{ns}$
$H^+$	0.982	75ns	184ns	0ns	69ns	163ns
$U^{28}$	0.568	130ns	159ns	61ns	120ns	189ns
$U^{73+}$	0.872	84ns	104ns	70ns	78ns	92ns

### 5.3.1 SIS18 extraction kicker units

Here we take three ion beams,  $H^+$ ,  $U^{28}$  and  $U^{73+}$ , to check the possibility, because the boundary ion species have the most stringent requirements. Fig. 5.11 shows three scenarios of the firing delay between two crates. Beam is firstly kicked by kicker units in the 1st crate and than kicked by the units in the 2nd crate to the transfer line. The yellow and red ellipse represents the position of the bunches, when the kicker units in the 1st and 2nd crate are fired. The number in the ellipse is used to tell different bunches. The head of the bunch is at the right side. The bunch 2 is firstly kicked. Here we assume ...the kicker units in the same crate are triggered instantaneous. The bunch gap is longer than ... d denotes the distance between two crates. L denotes the distance from the leftmost to the rightmost kicker unit. D denotes the sum distance of d and the 2nd crate. d equals to 19.167 meter. L equals to  $22.047\text{m} = d + 9 \times 0.25\text{m} + 7 \times 0.09\text{m}$ . D equals to  $20.437\text{m} = d + 4 \times 0.25\text{m} + 3 \times 0.09\text{m}$ .

Figure (a) is the easiest scenario. The kicker units in the 1st crate are fired when the tail of the bunch 1 passes by the 1st crate completely. The kicker units in the 2nd crate are fired when the tail of the bunch 1 passes by the 2nd crate completely. The delay for the firing two crates in this scenario is  $D/\beta c$ .  $\beta$  is ...

The second plot in Fig. 5.11 shows the scenario of the maximum delay between the firing of two crates. The kicker units in the 1st crate are fired when the tail of the bunch 1 passes by the 1st crate completely. The kicker units in the 2nd crate are fired 90ns before the head of the bunch 2 passes by it. The delay equals to  $G+d/\beta c-90\text{ns}$ .

The figure on the bottom shows the scenario of the minimum delay. The kicker units in the 1st crate are fired 90ns before the head of the bunch 2 passes by it. The kicker units in the 2nd crate are fired when the bunch 1 passes by the 2nd crate. The delay is  $L/\beta c-G+90\text{ns}$ .

Table 5.2 shows delay for three scenarios and related perimeters. The fixed delay is determined primarily by the boundary delay range from  $H^+$ ,  $U^{28}$  and  $U^{73+}$  beams, the delay range for other heavy ion species beams must be contained in these boundary range. According to the result, a fixed delay is available for firing kicker units in two crate for different beams. e.g. 80ns.

### 5.3.2 SIS100 injection kicker units

Two bunches from SIS18 will be continuously injected into one RF bucket after the other in SIS100. See Fig. 5.3. The yellow ellipse represents the circulating bunch in SIS100 and the red one represents the bunch to be injected. The head of the bunch is

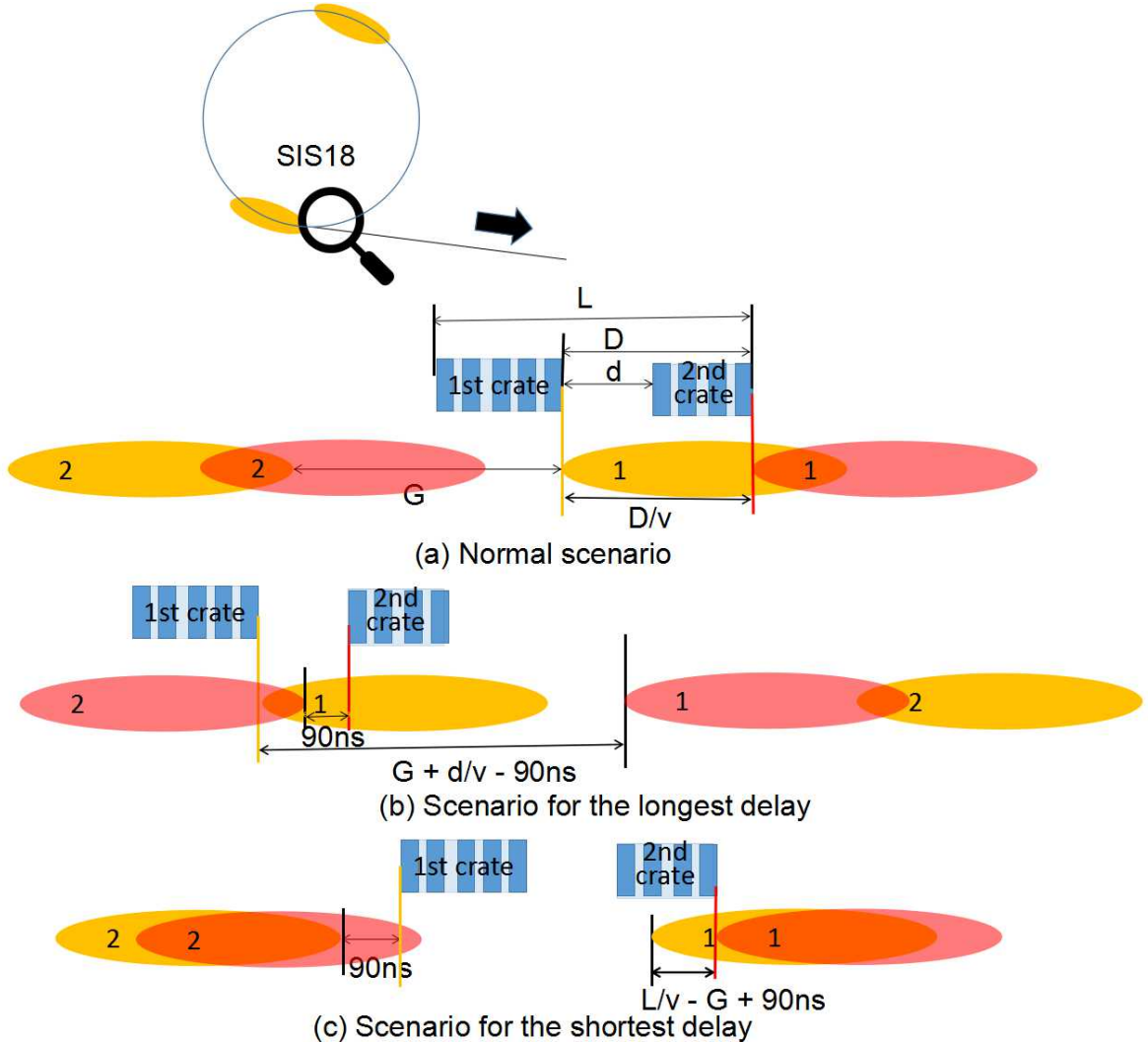


Abbildung 5.11: Three scenarios for the delay of SIS18 extraction kicker

at the left side. The preparation of the SIS100 injection kicker must be done during the bunch gap and it must be established for at least one SIS18 revolution period. For the instantaneous firing, all kicker units are fired only if the tail of the circulating bunch passes the leftmost kicker unit. The kicker pass time is the time needed for the tail of a bunch to pass from the rightmost unit to the leftmost kicker unit. The rise time of the kicker unit is 1/20 of the revolution period. Therefor the preparation time is the sum of the kicker pass time and rise time. The distance from the rightmost to the leftmost kicker unit is 3.79m,  $6 \times 0.22m + 5 \times 0.23m$ . If the preparation time is shorter than bunch gap, all kicker units could be fired instantaneous. Table 5.3 shows the preparation time for  $H^+$ ,  $U^{28}$  and  $U^{73+}$  beams and their bunch gap. The preparation time is much shorter than the bunch gap. So the kicker units could be fired instantaneous.

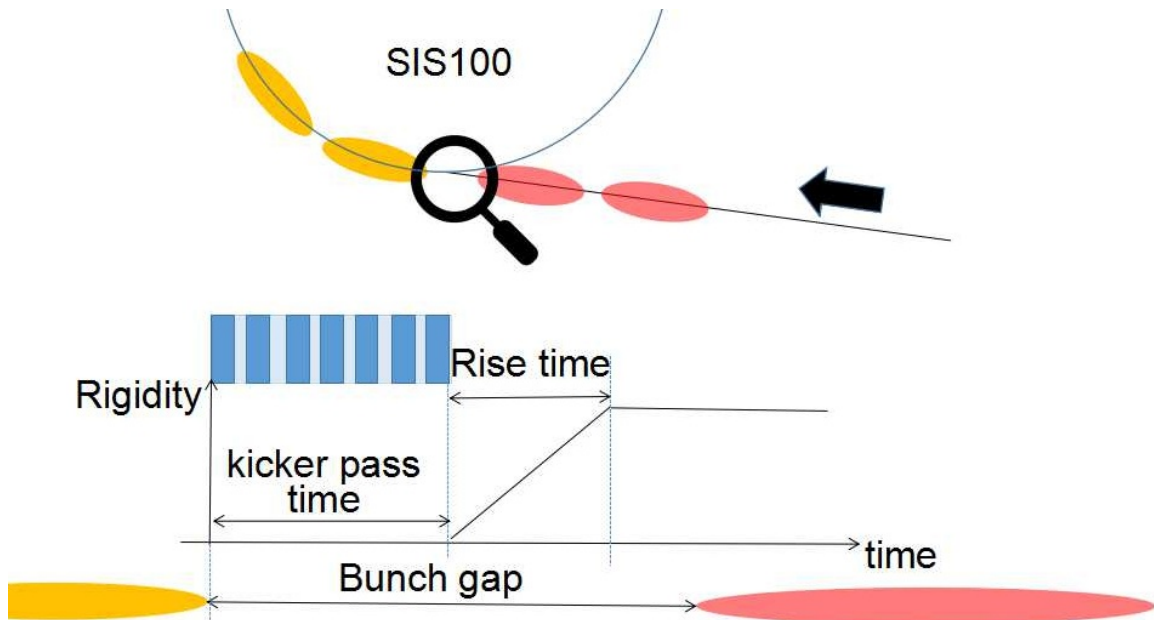


Abbildung 5.12: SIS100 injection kicker

Tabelle 5.3: The delay for firing SIS00 injection kicker

Beam	$\beta$	kicker pass time $L/\beta c$	Rise time $1/20 \times T_{rev}^{SIS100}$	Preparasion time $L/\beta c + 1/20 \times T_{rev}^{SIS100}$	bunch gap $2.25 \times T_{rev}^{SIS100}$
$H^+$	0.982	3ns	184ns	187ns	828ns
$U^{28}$	0.568	22ns	318ns	333ns	1431ns
$U^{73+}$	0.872	15ns	207ns	222ns	932ns

## 5.4 Test setup for the data collection, merging and redistribution of the B2B transfer system

### 5.4.1 Test requirement

The test setup achieves the following functional requirement.

- After receiving the B2B beginning event, both the B2B source and target SCUs collect predicted phase equivalent data from the source and target synchrotrons locally. The equivalence is a timestamp for the zero crossing point of the simulated RF reference signal.
- The B2B target SCU transfers the telegram containing the timestamp to the B2B source SCU.
- After receiving the data, the B2B source SCU calculates the synchronization window.
- The B2B source SCU sends the telegram containing the beginning of the synchronization window to the WR network.

- After receiving the telegram, the trigger SCU produces TTL output indicating the synchronization window.

### 5.4.2 Test setup introduction

Fig. 5.13 shows the schematic of the test setup. In this test setup, I use two MODEL DS345 Synthesized Function Generators with the frequency accuracy of  $\pm 5\text{ppm}$  of the selected frequency to simulate RF reference signals of SIS18 and SIS100. DS345 of SIS18 is directly triggered by the 10MHz of BuTiS receiver and DS345 of SIS100 is triggered by DS345 of SIS18. So both DS345s are synchronized to BuTiS. The B2B source SCU, B2B target SCU and trigger SCU are connected to the same WR switch, which connects to the WR network. PC is used to produce timing event and monitor the status of the B2B transfer programs in all SCUs. The oscilloscope is used to monitor the alignment of the two simulated RF reference signals within the synchronization window provided by the trigger SCU.

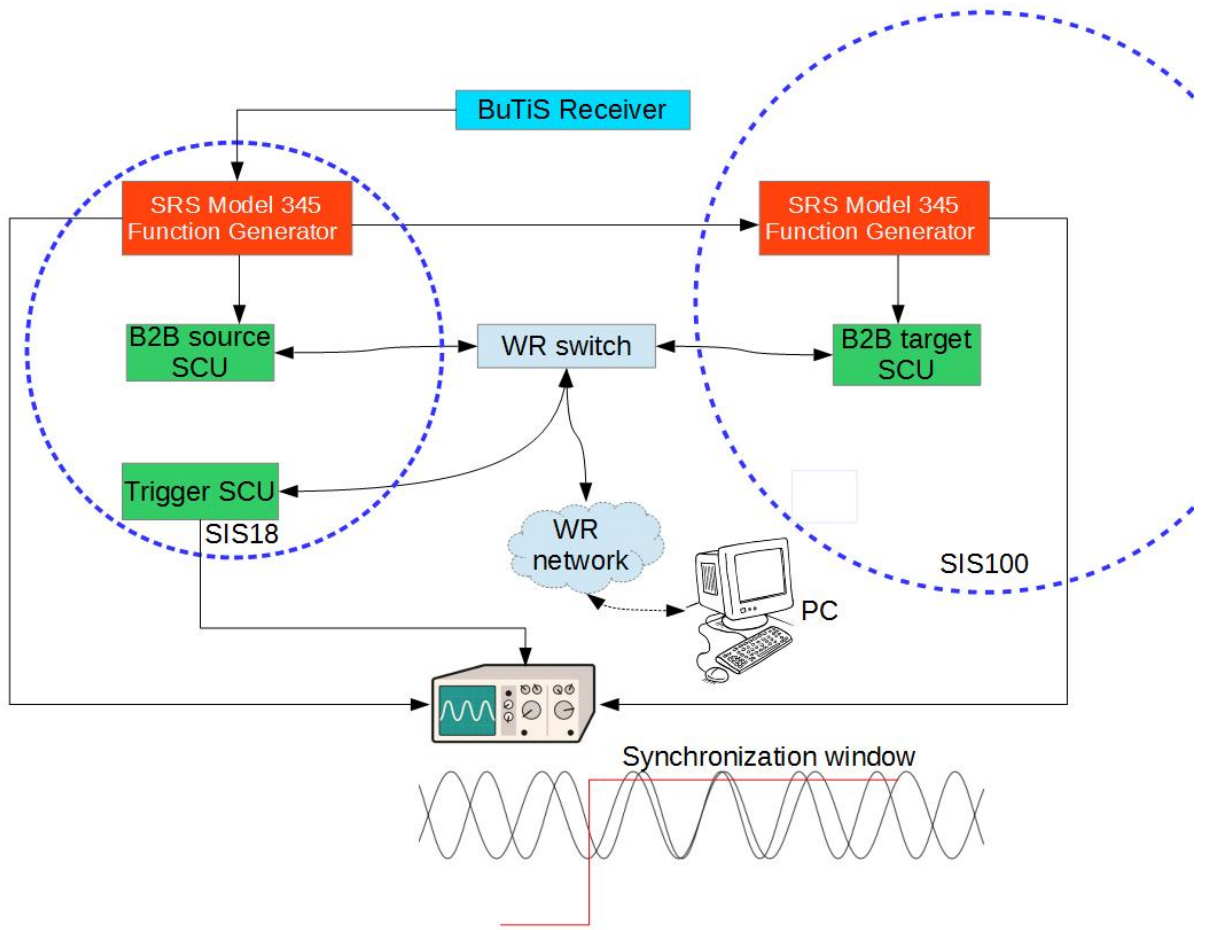


Abbildung 5.13: Schematic of the test setup

Fig. 5.14 shows the front and back view of the test setup. DS345 of SIS18 produces the sine wave of 1.572200MHz frequency for the B2B source SCU. DS345 of SIS100 produces the sine wave of 1.1572MHz for the B2B target SCU. So the beating frequency is 200Hz and the synchronization period is 5ms.

Fig. 5.15 shows the flow chart of the B2B programs running on the soft CPU LM32 of the B2B source.

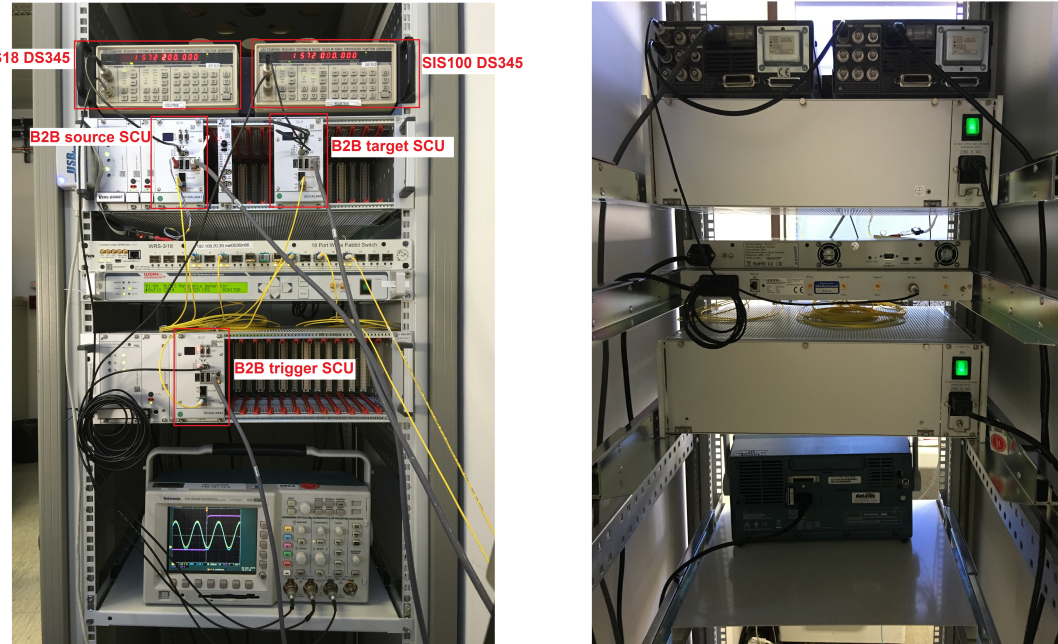


Abbildung 5.14: Test setup

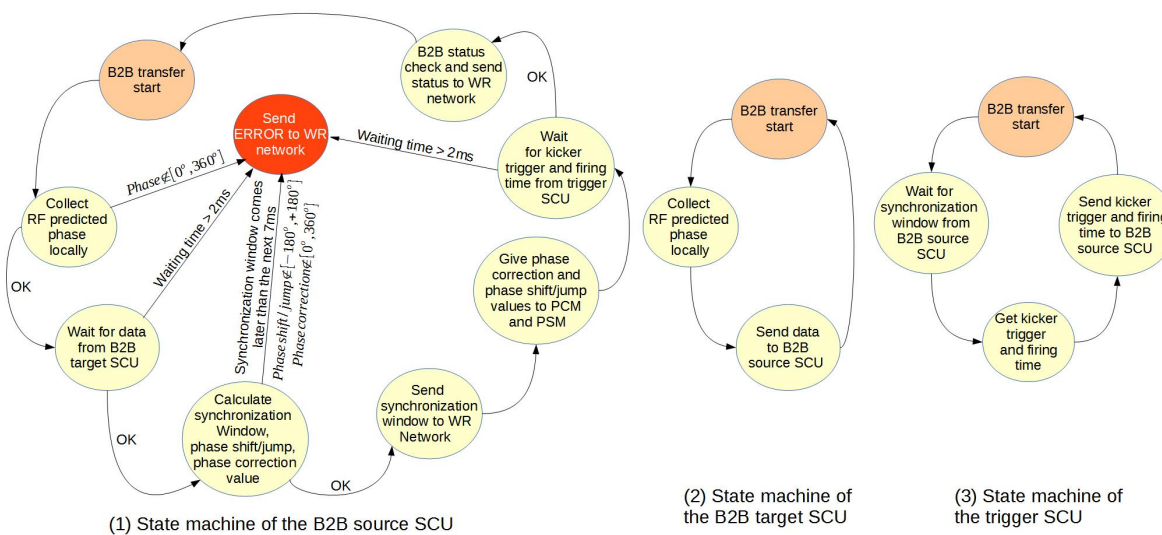


Abbildung 5.15: Flow chart of the B2B programs on SCUs.

Übersicht über SG an GSI, Aufbau, Funktionsweise

### 5.4.3 Test result

Fig. 5.16 shows status of the B2B programs on SCUs of the test setup.

Fig. 5.17 shows part of the SCU layout. The B2B event queue gets the B2B related telegrams at their absolute execution time. The timestamp zero-crossing points module is used to get the timestamp of the zero crossing point of the DS345 sine wave. The latching of the timestamp is triggered by LM32. The SCU slave interface supports the write and read between the LM23 and SCU slaves. LM32 of the B2B source and target SCUs are polling their B2B event queues. When they get

## **5KA DIESEL SET TRIPACATION AND A SYSTEMATION INVESTIGATION OF THE REDISTRIBUTION OF THE B2B TRANSFER SYSTEM**

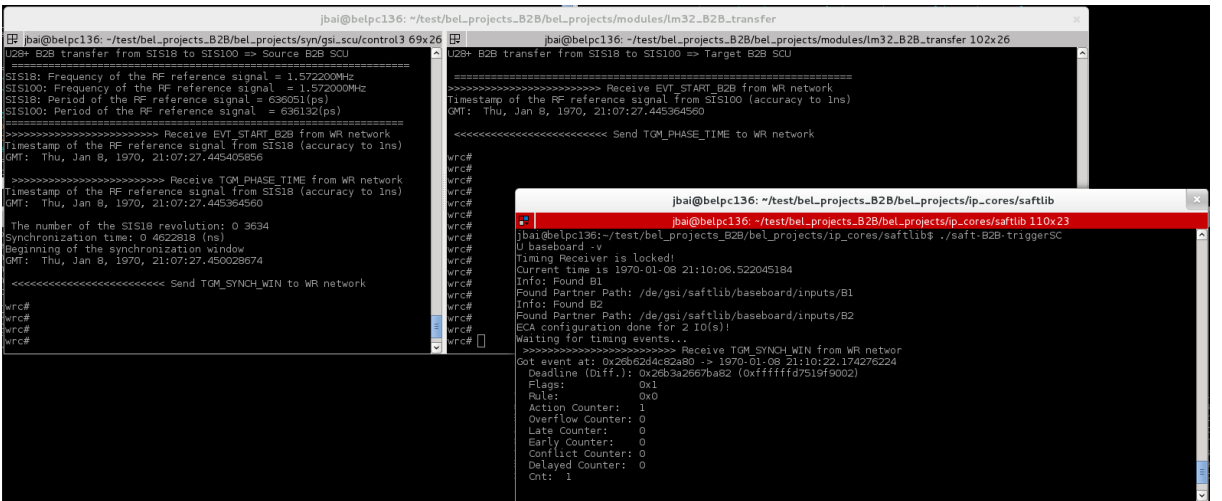


Abbildung 5.16: The result of the test setup

the B2B start event, they trigger the timestamp zero-crossing points module to latch timestamp. The asynchronous trigger is because of not only the non-real time of the program running on LM32, but also the block of the wishbone bus between top and dev crossbar by the monitor applications. So the B2B source and target SCU do not get the timestamp of the adjacent zero crossing points of two RF simulated sine signals in Fig. 5.16. In the test, the difference between two timestamps is 41.296us. The difference between timestamps of the adjacent zero crossing points, 592us, is the remainder resulting from 41.296us dividing SIS18 revolution period 636051ps. Based on the equation A and B, we could get the number of the SIS18 revolution period 3634 and the synchronization time 4.622818ms. For the real B2B transfer system, LM32 read the predicted phase from the PAP module when it polls the B2B start event. Only LM32 is allowed to use the wishbone bus between top and dev crossbars. The asynchronous reading is only caused by the non-real time LM32 program, which is around 1us. For the PAP module, the predicted phase is constant for 9us.

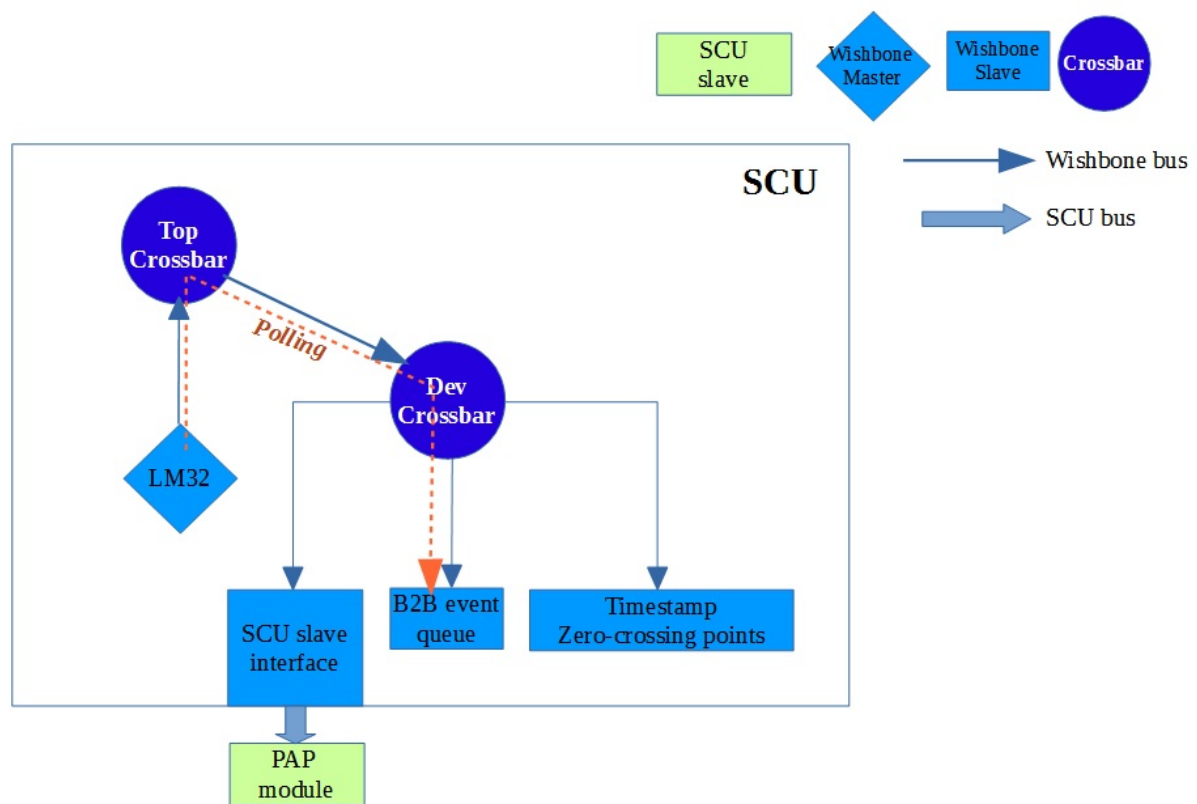


Abbildung 5.17: Topology of the SCU.

# Kapitel 6

## Existing transfer system and the transfer system of the FAIR accelerators

- 6.1 Existing transfer from SIS18 to ESR
- 6.2 B2B transfer from SIS18 to ESR to CRY-RING

# Kapitel 7

## Summary

# Kapitel 8

## Acknowledgement

I wish to express my sincere gratitude to Prof. Oliver Kester, David Ondreka and Dietrich Beck for their supervision, valuable guidance and helpful suggestions. I would like to express my sincere appreciation to Turgut «elikadam, for providing us VoIP device for our measurements. He also helped us for adding extra functions for delay measurements to VoIP device. And also I want to thank to Hasan «itÁ and my friends in ASELSAN Inc. for their valuable friendship, help and support. I want to thank to Şanser Şirin from Hacettepe University and Oktay KoÁ from Middle East Technical University for their help and support during measurements. And also I want to thank to Mehmet Celep, Alparslan G^zel and Halil İbrahim Seyrek from Gebze Institute of Technology for their help and support during measurements. I am also grateful to ASELSAN Inc. for facilities provided for the completion of this thesis. I am grateful to my wife, Esin, because she always supported me and cheered me up when I needed.

# Kapitel 9

## References

# Anhang A

## Formelzeichen

### A.1 Konstanten

1. Elementarladung

$$1e = 1,6021766208(98) * 10^{-19} C$$

2. nächstes Geraffel

## **Anhang B**

### **Messwerttabellen**

## **Anhang C**

### **Abbildungsverzeichnis**